Spin-valley polarized quantum anomalous Hall effect and a valley-controlled half-metal in bilayer graphene

Zhai, Xuechao; Blanter, Yaroslav M.

Important note
To cite this publication, please use the final published version (if applicable).
Please check the document version above.

Spin-valley polarized quantum anomalous Hall effect and a valley-controlled half-metal in bilayer graphene

Xuechao Zhai [1,2,*] and Yaroslav M. Blanter[2,†]

[1]*New Energy Technology Engineering Laboratory of Jiangsu Province & Institute of Information Physics, School of Science, Nanjing University of Posts and Telecommunications (NJUPT), Nanjing 210023, China*
[2]*Kavli Institute of NanoScience, Delft University of Technology, 2628 CJ Delft, The Netherlands*

We investigate topological phases of bilayer graphene subject to antiferromagnetic exchange fields, interlayer bias, and light irradiation. We discover that at finite bias and light intensity the system transitions into a previously unknown spin-valley polarized quantum anomalous Hall (SVP-QAH) insulator state, for which the subsystem of one spin is a valley Hall topological insulator (TI) and that of the other spin is a QAH insulator. We assess the TI phases occurring in the system by analytically calculating the spin-valley-dependent Chern number and characterize them by considering edge states in a nanoribbon. We demonstrate that the SVP-QAH edge states lead to a unique spin rectification effect in a domain wall. Along the phase boundary, we observe a bulk half-metal state with Berry's phase of 2π.

I. INTRODUCTION

Bernal-stacked bilayer graphene (BLG) consists of two honeycomb lattices coupled by van der Waals interaction [1]. Due to its novel electronic properties, such as low-energy states with Berry's phase of [2] 2π and an electrically tunable band gap [3,4], BLG has recently attracted much attention both theoretically and experimentally, see, e.g., Refs. [5–10]. In particular, BLG became popular for studies of phenomena related to the valley degree of freedom [9,11–14], resulting in discovery of nontrivial topological states of matter. Recently, a striking finding was the discovery of the quantum valley Hall (QVH) effect in BLG, for which the edge states in the gap driven by an interlayer bias are valley polarized and provide the conductance quantization with the step of [15–18] $4e^2/h$. Theoretical studies have predicted that the usual QVH insulator in BLG undergoes a transition to a valley-polarized quantum spin Hall insulator under effect of Rashba spin-orbit interaction [19,20].

Another attractive topological state of matter is the quantum anomalous Hall (QAH) state, generally characterized by chiral edge states in the gap and nonzero charge Chern numbers [21–23]. The QAH state in BLG has been suggested to be induced by Rashba interaction and internal magnetization [24] or by strong circularly polarized light [25–27], different from the mechanism of Landau-level quantization in the quantum Hall effect. Most recently, the valley-polarized QAH state possessing the properties of both the QVH and QAH states has been proposed in other two-dimensional

(2D) systems [28,29], similar to BLG. Interestingly, this QAH state can possess edge states which are not complectly chiral [28].

In this work, we present the light- and voltage-controlled phase diagram of BLG in contact with a layered antiferromagnetic (LAF) exchange field and discover a variety of topological insulator (TI) states in this system. We argue that this antiferromagnetic BLG itself is a quantum anomalous valley Hall (QAVH) insulator [30], that it undergoes a transition to a usual QVH insulator as interlayer bias increases, and that it is switched to a normal QAH (N-QAH) insulator, a system with chiral edge states, as light intensity increases. Remarkably, we discover that if both voltage and light are applied, the system can be in a spin-valley polarized QAH (SVP-QAH) insulator state, for which the subsystem of one spin is in a QVH state and that of the other spin is in a QAH state. To our knowledge, this state has not been previously described in the literature, and it is distinct from the single-valley spin-polarized QAH states [26,29] and the QAH states with no spin or valley polarizations [13–17,21–23,28].

The TI states in the system are discriminated by the spin-valley-dependent Chern number [9], which we calculate analytically. We further characterize these TIs by edge states in a zigzag ribbon and show transport differences in domain walls (DWs). In the phase boundary, we discover that the 2D bulk system can host a half-metal state with Berry's phase of 2π, and the number of gap-closing valleys is tunable.

Our paper is organized as follows. In Sec. II, we introduce the system Hamiltonian and topological theory. In Sec. III, we show the phase diagram and give the low-energy formalism. In Sec. IV, we analytically derive the Chern numbers and show the DW transport. In the final section, we present the Discussion and Conclusions.

*zxc@njupt.edu.cn
†Y.M.Blanter@tudelft.nl

II. SYSTEM HAMILTONIAN AND TOPOLOGICAL THEORY

The BLG system we consider is described by the eight-band tight-binding model,

$$
\hat{H} = -J \sum_{\langle i,j \rangle_{\parallel} \alpha} c_{i\alpha}^{\dagger} c_{j\alpha} - \gamma \sum_{\langle i,j \rangle_{\perp} \alpha} c_{i\alpha}^{\dagger} c_{j\alpha} + M \sum_{i\alpha} \mu_i c_{i\alpha}^{\dagger} \sigma_z c_{i\alpha}
$$

$$
- U \sum_{i\alpha} \mu_i c_{i\alpha}^{\dagger} c_{i\alpha} + i \frac{\lambda}{3\sqrt{3}} \sum_{\langle\langle i,j \rangle\rangle_{\parallel} \alpha} \nu_{ij} c_{i\alpha}^{\dagger} c_{j\alpha}, \quad (1)
$$

where $c_{i\alpha}^{\dagger}$ creates an electron with spin polarization α at site i, and $\langle i,j \rangle / \langle\langle i,j \rangle\rangle$ run over all the nearest and next-nearest-neighbor hopping sites. The subscript $\parallel$ ($\perp$) denotes "in plane" ("out of plane"), $\mu_i = \pm 1$ indicates that site i lies in the bottom (top) layer, σ_z is the z component of Pauli matrix in the spin subspace, and $\nu_{ij} = +1 (-1)$ holds if the next-nearest hopping is anticlockwise (clockwise). In Eq. (1), the first and second terms are the intralayer and interlayer nearest-neighbor hoppings with [8] $J = 3.0$ eV and $\gamma = 0.39$ eV. The third term, H_M, is the LAF exchange field, which can be applied by depositing BLG between 2D magnetic insulators CrI₃ [30] ($M \sim 7$ meV can be achieved). The fourth term, H_U, is the interlayer bias, with U being up to 125 meV in the experiment [4,7]. The fifth term, H_{λ}, is the Haldane mass term [31], which can be applied [26] by irradiating BLG with circularly polarized light (see Supplemental Material (SM) [32] and Refs. [33,34]). Estimated from the bandwidth in BLG, the light frequency would typically lie in the range [26,32] 10^{13}–10^{14} Hz, leading to the estimate of $\lambda \sim 10$ meV.

The QAH effect is characterized by the charge Chern number [21–24,28],

$$
C = \frac{1}{2\pi} \sum_n \int_{BZ} d^2\mathbf{k}\, \Omega_n(\mathbf{k}), \quad (2)
$$

where Ω_n is the momentum-space Berry curvature [9] in the out-of-plane direction for the nth subband

$$
\Omega_n(\mathbf{k}) = -\sum_{n' \neq n} \frac{2\mathrm{Im}\langle \psi_{nk}|\upsilon_x|\psi_{n'k}\rangle\langle \psi_{n'k}|\upsilon_y|\psi_{nk}\rangle}{(\varepsilon_{n'} - \varepsilon_n)^2}. \quad (3)
$$

The summation is over all occupied valence bands in the first Brillouin zone below the bulk band gap, ψ is the Bloch state, and $\upsilon_{x(y)}$ is the velocity operator along the $x(y)$ direction.

One can label a state a TI if it has at least one nonzero topological invariant [24–27,29–31,33,34]. Because electrons in BLG here have a mixture of charge, spin, and valley degrees of freedom, the index C cannot identify the spin- or valley-polarized TI phases. To solve this problem, we employ a decomposed, spin- and valley-dependent Chern number [9,34] C_{η}^s, which is well defined in half of the first Brillouin zone around K ($\eta = +1$) or K' ($\eta = -1$) points for spin-up ($s = +1$) or spin-down ($s = -1$) electrons. On the basis of C_{η}^s, the spin and valley Chern numbers [9] can be defined as $C_S = C_{\uparrow} - C_{\downarrow} = \sum_{\eta}(C_{\eta}^{\uparrow} - C_{\eta}^{\downarrow})$ and $C_{\upsilon} = C_K - C_{K'} = \sum_s (C_K^s - C_{K'}^s)$, respectively. The charge Chern number satisfies $C = \sum_{\eta,s} C_{\eta}^s$.
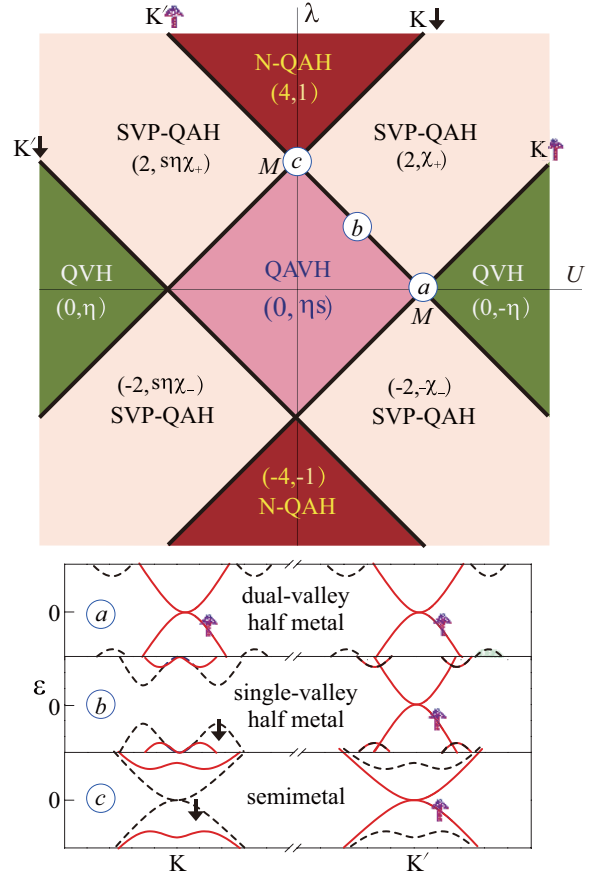

FIG. 1. Phase diagram in the U-λ plane (top). The Chern numbers (C, C_{η}^s) are used to index the TI phases. For the SVP-QAH state, $C_{\eta}^s = \chi_{\pm} = (\delta_{s,1} + \delta_{s,-1})(\delta_{s,1} \pm s\eta\delta_{s,-1})$ [see Eq. (11)]. Bold lines represent the phase boundaries, where gap closing is indexed by K (K') and $\uparrow$ ($\downarrow$). The bulk bands for points a–c are shown at the bottom, where solid (dashed) lines denote $\uparrow$ ($\downarrow$) subbands.

III. PHASE DIAGRAM AND LOW-ENERGY FORMULISM

We present our result as the phase diagram in Fig. 1 by tuning U and λ. The topological numbers (C, C_{η}^s) are used to index the TI phases, including QAVH, QVH, N-QAH, and SVP-QAH. We show how to derive the analytical expressions for the phase boundary and the Chern numbers from low-energy theory later. Because the sign changes of U and λ only influence the signs of Chern numbers (no novel phases appear), one only needs to characterize the phases for ($U \geqslant 0$, $\lambda \geqslant 0$). To describe the edge states, some typical cases are chosen to calculate the bands in a zigzag ribbon (SM [32]). The edge states in real space for each TI are illustrated in Figs. 2(a)–2(d), where the moving directions (hollow arrows) for electrons agree with Eqs. (9)–(12). At the phase boundary, the bulk gap closes Eq. (6).

We first discuss the QAVH state, for which $(C, C_{\eta}^s) = (0, \eta s)$ [30]. The nonzero value of C_{η}^s in this phase arises from the inversion symmetry breaking dominated by M. Although the QAVH phase has metallic in-gap edge states near K and K', the index C is zero. The anomalous property of the state is that the subsystem of each spin is a QVH insulator [$C_{\upsilon}^{\uparrow} = C_K^{\uparrow} - C_{K'}^{\uparrow} = C_{K'}^{\downarrow} - C_K^{\downarrow} = -C_{\upsilon}^{\downarrow} = 2$ in Fig. 2(a)], while
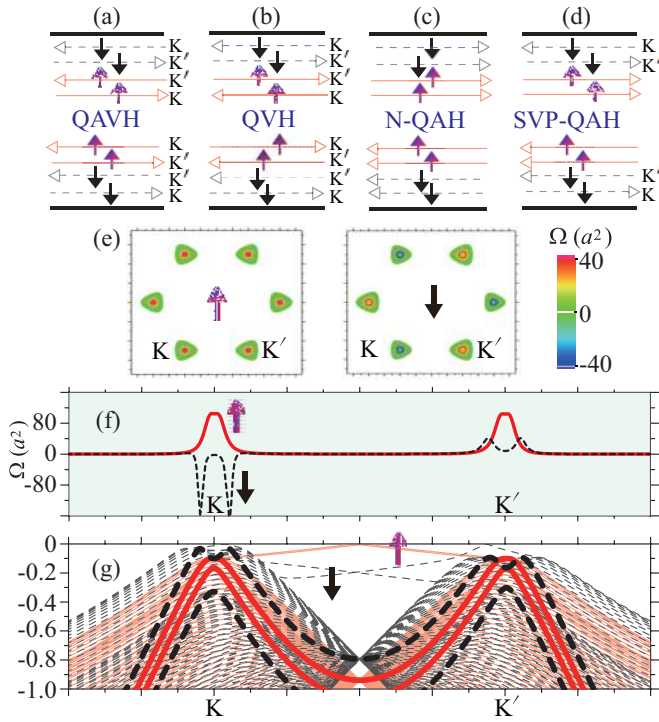
FIG. 2. (a)–(d) Schematics of eight edge states in the bulk gap for four TIs in Fig. 1, corresponding to our calculated band structures [32] of a zigzag-edged ribbon for typical points under $(U \geqslant 0, \lambda \geqslant 0)$. (e)–(g) Electronic properties of the SVP-QAH state. Berry curvature in (e) (k_x, k_y) plane and (f) along K-K' direction, corresponding to (g) the bulk (thick lines) and ribbon (thin lines) bands.

the whole system is not valley polarized ($C_v = 0$). The result $C_K^{\uparrow} + C_K^{\downarrow} = C_{K'}^{\uparrow} + C_{K'}^{\downarrow} = 0$ indicates the edge states in each valley behave as a quantum spin Hall state [19,22] in spite of $C_S = 0$. If we include nonzero voltage U, the system eventually undergoes a transition to a normal QVH insulator [$C_v = -4$ in Fig. 2(b)] due to the competition of U and M. The QAVH insulator transitions to an N-QAH insulator [$C = 4$ in Fig. 2(c)] as λ increases due to the time-reversal symmetry breaking. Each transition is associated with with a process of the closing and reopening of the gap.

Our most significant result is the SVP-QAH phase, which appears in regions where $U\lambda \neq 0$ and occupies a major part of the phase diagram. For a SVP-QAH state, four spin-down edge states in the gap appear near K and K', but four spin-up edge states appear away from K and K' [Figs. 2(d) and 2(g)]. Correspondingly, the Berry curvature in the (k_x, k_y) plane [Fig. 2(e)] and specifically along the K-K' direction [Fig. 2(f)] is shown. We find that the spin-down subsystem is a QVH insulator [$C_K^{\downarrow} = -C_{K'}^{\downarrow} = -1, C_v^{\downarrow} = -2, C^{\downarrow} = C_K^{\downarrow} + C_{K'}^{\downarrow} = 0$], whereas the spin-up subsystem is a normal QAH insulator [$C_K^{\uparrow} = C_{K'}^{\uparrow} = 1, C_v^{\uparrow} = 0, C^{\uparrow} = C_K^{\uparrow} + C_{K'}^{\uparrow} = 2$], and then $C = -C_v = C_S = 2$ is achieved. This SVP-QAH insulator is a type of QAH state which differs obviously from the single-valley spin-polarized QAH [26,29], spin-unpolarized QAH [9,12–14,28], and valley-unpolarized QAH [9,22,34] states discovered previously.

At the phase boundaries, see bold lines in Fig. 1, there exists a 2D bulk state that is half-metallic [35] (gap closing at K or K'), as shown by the completely spin-polarized band structures (bottom) near the Fermi level for the marked points a and b. In contrast, point a corresponds to a dual-valley half-metal (valley degeneracy), while point b refers to a single-valley half-metal (the other valley is insulating). For the marked point c, spin-down (spin-up) subbands near the Fermi level are locked to the K (K') valley, resulting in a spin-valley locked semimetal. Thus gap closing of the valleys occurs in which one or two is tunable. Notably, the bulk half-metal state here has the Berry's phase of 2π Eq. (8).

To further explore the physics underlying the phase diagram, we analyze the low-energy effective Hamiltonian derived from the lattice model (1) after Fourier transformation and reveal the physics of electrons near K and K'. For simplicity, we set $\hbar = 1$ and $v_F = 1$ below. Because two opposite spins are decoupled in Eq. (1), the effective Hamiltonian can be written as a 4×4 matrix,

$$\mathcal{H}_k = \begin{pmatrix} \Delta_{\eta s}^{+} - U, & \eta k_x - i k_y, & 0, & 0 \\ \eta k_x + i k_y, & -\Delta_{\eta s}^{-} - U, & -\gamma, & 0 \\ 0, & -\gamma, & \Delta_{\eta s}^{-} + U, & \eta k_x - i k_y \\ 0, & 0, & \eta k_x + i k_y, & -\Delta_{\eta s}^{+} + U \end{pmatrix},$$

(4)

where $\Delta_{\eta s}^{\pm} = \eta\lambda \pm sM$. Note that s and M only occur as a product sM, and thus the reversal of the sign of M is equivalent to the reversal of spin orientation. We will assume $M > 0$. By matrix diagonalization, we derive the band structure as

$$\varepsilon = \pm\sqrt{k^2 + (sM - U)^2 + \lambda^2 + \tfrac{1}{2}(\gamma^2 \pm \sqrt{\Gamma_k})},$$

$$\Gamma_k = k^2[16(sM - U)^2 + 4\gamma^2] + [\gamma^2 - 4\eta\lambda(sM - U)]^2.$$

(5)

Note that the electron-hole symmetry is present in Eq. (5), from which one can prove that the gap is closed only under $\varepsilon = 0$, which requires $k = 0$ [at $K(K')$] and simultaneously,

$$U = sM + \eta\lambda.$$

(6)

According to the topological theory [9], this gap-closing condition in Eq. (6) precisely describes the phase boundary as given in Fig. 1. Specifically, at $k = 0$, the energy gap reads

$$\Delta_{\eta}^{s} = 2\sqrt{(sM - U)^2 + \lambda^2 + \tfrac{1}{2}\left(\gamma^2 - |\gamma^2 - 4\eta\lambda(sM - U)|\right)}.$$

(7)

Judging from Eq. (6), the system is a dual-valley half-metal for $(\lambda, U) = (0, \pm M)$ and a spin-valley locked semimetal for $(\lambda, U) = (\pm M, 0)$. Except for these points, the system is a single-valley half-metal in the phase boundary. The effective 2×2 Hamiltonian used in Ref. [2] can be derived to describe the low-energy half-metal subbands with parabolic dispersion. The half-metal Bloch state $\psi_{k,\phi}$ (ϕ being the azimuthal angle of the momentum) here has the Berry phase [36]

$$\varphi_B = i \int_0^{2\pi} d\phi \langle \psi_{k,\phi} | \frac{\partial}{\partial \phi} | \psi_{k,\phi} \rangle = 2\eta\pi,$$

(8)

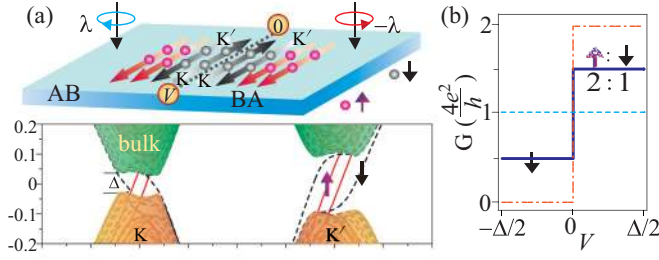which can induce a spin-polarized integer quantum Hall effect with a missing zero-level plateau [2].

FIG. 3. (a) Sketch of a DW (top) between AB- and BA-stacked BLG. The voltage V (0) is for detection. The conducting channels are shown for the AB(λ)/BA($-\lambda$) case, with the band (bottom) given in a sharp DW. The band gap satisfies $\Delta \simeq \min\Delta_\eta^s(\eta, s = \pm1)$. (b) DW conductance within the gap in the AB(λ)/BA($-\lambda$) DWs. The solid, dashed, and dot-dashed lines represent, respectively, the SVP-QAH, QAVH (the same for QVH), and N-QAH cases.

IV. CHERN NUMBERS AND DOMAIN-WALL TRANSPORT

We see from Eq. (6), Fig. 1, and our band calculations [32] that the QAVH, QVH, N-QAH, and SVP-QAH insulator states hold under $|\lambda| < M - |U|$, $|\lambda| < |U| - M$, $|\lambda| > |U| + M$, $||U| - M| < |\lambda| < |U| + M$, respectively. Usually, the topological invariants are associated with the signs of the parameters for a TI state [9,34]. For the QAVH, QVH, and N-QAH insulators here, the index C_η^s is respectively determined by

$$C_\eta^s = \eta s, \ -\eta\,\mathrm{sgn}(U), \ \mathrm{sgn}(\lambda), \qquad (9)$$

and correspondingly, C, C_S, C_υ are expressed as

$$C = 0, 0, \ 4\mathrm{sgn}(\lambda) \parallel C_S = 0, 0, 0 \parallel C_\upsilon = 0, -4\mathrm{sgn}(U), 0, \tag{10}$$

where $\mathrm{sgn}(x)$ is the sign function. For the SVP-QAH insulator, we calculate C_η^s to be

$$C_\eta^s = (\delta_{s,1} + \delta_{s,-1})[\mathrm{sgn}(\lambda)\delta_{s,\mathrm{sgn}(U)} + s\eta\delta_{s,\mathrm{sgn}(-U)}], \tag{11}$$

and the other Chern numbers satisfy

$$C = 2\mathrm{sgn}(\lambda), \ C_s = 2\mathrm{sgn}(\lambda U), \ C_\upsilon = -2\mathrm{sgn}(U). \tag{12}$$

Here, $\delta_{\mu,\nu}$ is the Kronecker δ function. We see from Eqs. (9) and (11), $|C_\eta^s| = 1$ always holds for each TI case.

To distinguish and detect the SVP-QAH state, we consider a DW between AB- and BA-stacked BLG [15] in Fig. 3(a), where the conducting channels and band structure are shown when λ has the opposite values in AB and BA regions. By using the Green's function method [37], we show the DW conductance [$G = I/V$, where $I(V)$ is the current (bias)] in Fig. 3(b) and predict a unique spin rectification effect (solid line) for the SVP-QAH edge states. We assume here that the DW is much shorter than the electron mean free path, and thus scattering is ignored. The ratio of channel numbers for ↑ and ↓ is 2 : 1 for $V > 0$, while only ↓ channels contribute to transport for $V < 0$. In contrast, no charge or spin rectifications occur for the QAVH or QVH states. The N-QAH state acts as a charge diode; however, still no spin rectification occurs.

The spin/valley filter or diode can be further realized by tuning the types of DW and fields (SM [32]). Specifically, a unipolar spin diode [38] (only spin-up electrons are unidirectionally conducting) works if the DW in Fig. 3(a) is

of the armchair type due to the absence of the QVH edge states [9–12].

V. DISCUSSION AND CONCLUSIONS

Realization of the SVP-QAH state in BLG depends strongly on the LAF field, H_M, which is not induced by the electron-electron interaction [26] but by proximity, such as a van der Waals system consisting of BLG and magnetic insulator CrI_3 [30] ($M \sim 7$ meV can be achieved). Possibilities of proximity induced by other 2D magnets, such as $CrBr_3$ or $Cr_2Ge_2Te_6$ [39], require more research. The magnetic insulator EuS is an alternative candidate to induce H_M on the basis of relevant experimental evidence [40]. Beyond model (1), the Coulomb interaction might induce a gap of about 1 meV [7,26], which is usually disregarded when other interactions are stronger [4,15–17] as we assume. Notably, the LAF order cannot be easily broken by light in spite of magneto-optical Kerr or spin-phonon coupled effects [41,42]. If the LAF system becomes ferromagnetic, e.g., by applying magnetic field [30], the SVP-QAH phase disappears.

In particular, the time-periodic optical field can be safely reduced to the time-averaged static term H_λ under high-frequency ($> 3J$) conditions [25–27,34], when the Chern number is well defined to characterize the quantized current [43–45] of edge states near $E = 0$. This is further carefully checked (SM [32]) by using the full-time Floquet theory. Because the light absorbance per graphene layer is only about 2.3% [46], the band population is presumably intact. For the SVP-QAH DW transport in Fig. 3(a), the electron mean free path $L_0 \sim 420$ nm was found by experiment [15–18]. Ignoring the contact resistance, the dependence of ballistic conductance G on DW length L reads [15,37] $G = (\zeta e^2/h)(1 + L/L_0)$, where ζ is the integer for quantized plateau in Fig. 3(b). For the lower-frequency light, other complex effects such as [47–49] time-averaged densities of states in addition to edge states can break the conductance quantization [32].

The exchange proximity effect in a graphene/2D magnet may be rather small so that pressure is usually needed to induce a measurable QAH effect [50]. Certainly, small details related to the physics close to the Fermi level, such as band hybridization, charge transfer, exchange proximity or bias effects, may change the phase diagram at the level of *ab initio* calculations [30], reduce the conductivity, and even hamper the observation of the SVP-QAH phase. Therefore, more efforts both in theory and experiment are still needed to explore and confirm the SVP-QAH phase in BLG/2D-magnet systems.

Another striking result revealed by Eq. (11) is that, without optical fields, the SVP-QAH phase holds in systems with intrinsic spin-orbit coupling (by replacing H_λ with sH_λ). A promising alternative system to obverse the SVP-QAH phase is the experimentally available LAF Eu/bilayer silicene/Eu structure [51]. Our further calculations [32] indicate the SVP-QAH is robust against weak Rashba interactions.

In summary, the concept of van der Waals LAF order applied to 2D valleytronics, rarely noticed before, opens an avenue for engineering small devices with ultralow dissipation. The explored topological transitions modulated by photon and

electric voltage will motivate the experimental exploration of novel 2D QAH insulators with rich spin or valley physics in the integrated systems between layered 2D materials, van der Waals magnets, and correlated valley materials, for which the combination of spintronics, valleytronics, and topology promises discoveries of unique condensed matter phases.

ACKNOWLEDGMENTS

[1] T. Ohta, A. Bostwick, T. Seyller, K. Horn, and E. Rotenberg, Science **313**, 951 (2006).

[2] K. S. Novoselov, E. McCann, S. V. Morozov, V. I. Fal'ko, M. I. Katnelson, U. Zeitler, D. Jiang, F. Schedin, and A. K. Geim, Nat. Phys. **2**, 177 (2006).

[3] E. McCann, Phys. Rev. B **74**, 161403(R) (2006).

[4] Y. Zhang, T.-T. Tang, C. Girit, Z. Hao, C. C. Martin, A. Zettl, M. F. Crommie, Y. R. Shen, and F. Wang, Nature (London) **459**, 820 (2009).

[5] I. Martin, Y. M. Blanter, and A. F. Morpurgo, Phys. Rev. Lett. **100**, 036804 (2008).

[6] R. T. Weitz, M. T. Allen, B. E. Feldman, J. Martin, and A. Yacoby, Science **330**, 812 (2010).

[7] J. Velasco Jr., L. Jing, W. Bao, Y. Lee, P. Kratz, V. Aji, M. Bockrath, C. N. Lau, C. Varma, R. Stillwell, D. Smirnov, F. Zhang, J. Jung, and A. H. MacDonald, Nat. Nanotechnol. **7**, 156 (2012).

[8] E. McCann and M. Koshino, Rep. Prog. Phys. **76**, 056503 (2013).

[9] Y. Ren, Z. Qiao, and Q. Niu, Rep. Prog. Phys. **79**, 066501 (2016).

[10] L. Ju, L. Wang, T. Cao, T. Taniguchi, K. Watanabe, S. G. Louie, F. Rana, J. Park, J. Hone, F. Wang, and P. L. McEuen, Science **358**, 907 (2017).

[11] W. Jaskólski, M. Pelc, G. W. Bryant, L. Chico, and A. Ayuela, 2D Mater. **5**, 025006 (2018).

[12] F. Zhang, A. H. MacDonald, and E. J. Mele, Proc. Natl. Acad. Sci. **110**, 10546 (2013).

[13] F. Zhang, J. Jung, G. A. Fiete, Q. Niu, and A. H. MacDonald, Phys. Rev. Lett. **106**, 156801 (2011).

[14] X. Li, F. Zhang, Q. Niu, and A. H. MacDonald, Phys. Rev. Lett. **113**, 116803 (2014).

[15] L. Ju, Z. Shi, N. Nair, Y. Lv, C. Jin, J. Velasco Jr, C. Ojeda-Aristizabal, H. A. Bechtel, M. C. Martin, A. Zettl, J. Analytis, and F. Wang, Nature (London) **520**, 650 (2015).

[16] J. Li, K. Wang, K. J. McFaul, Z. Zern, Y. Ren, K. Watanabe, T. Taniguchi, Z. Qiao, and J. Zhu, Nat. Nanotechnol. **11**, 1060 (2016).

[17] L.-J. Yin, H. Jiang, J.-B. Qiao, and L. He, Nat. Commun. **7**, 11760 (2016).

[18] L. Jiang, Z. Shi, B. Zeng, S. Wang, J.-H. Kang, T. Joshi, C. Jin, L. Ju, J. Kim, T. Lyu, Y.-R. Shen, M. Crommie, H.-J. Gao, and F. Wang, Nat. Mater. **15**, 840 (2016).

[19] Z. Qiao, W.-K. Tse, H. Jiang, Y. Yao, and Q. Niu, Phys. Rev. Lett. **107**, 256801 (2011).

[20] X. Zhai and G. Jin, Phys. Rev. B **93**, 205427 (2016).

[21] C.-Z. Chang, J. Zhang, X. Feng, J. Shen, Z. Zhang, M. Guo, K. Li, Y. Ou, P. Wei, L.-L. Wang, Z.-Q. Ji, Y. Feng, S. Ji, X. Chen, J. Jia, X. Dai, Z. Fang, S.-C. Zhang, K. He, Y. Wang *et al.*, Science **340**, 167 (2013).

[22] M. Ezawa, Phys. Rev. Lett. **109**, 055502 (2012).

[23] X. Zhai and G. Jin, Phys. Rev. B **89**, 235416 (2014).

[24] W.-K. Tse, Z. Qiao, Y. Yao, A. H. MacDonald, and Q. Niu, Phys. Rev. B **83**, 155447 (2011).

[25] P. Mohan and S. Rao, Phys. Rev. B **98**, 165406 (2018).

[26] C. Qu, C. Zhang, and F. Zhang, 2D Mater. **5**, 011005 (2018).

[27] V. Dal Lago, E. Suarez Morell, and L. E. F. Foa Torres, Phys. Rev. B **96**, 235409 (2017).

[28] H. Pan, Z. Li, C.-C. Liu, G. Zhu, Z. Qiao, and Y. Yao, Phys. Rev. Lett. **112**, 106802 (2014).

[29] J. Zhou, Q. Sun, and P. Jena, Phys. Rev. Lett. **119**, 046403 (2017).

[30] C. Cardoso, D. Soriano, N. A. García-Martínez, and J. Fernández-Rossier, Phys. Rev. Lett. **121**, 067701 (2018).

[31] F. D. M. Haldane, Phys. Rev. Lett. **61**, 2015 (1988).

[32] See Supplemental Material http://link.aps.org/supplemental/10.1103/PhysRevB.101.155425 for details on the item H_λ, the bands in a zigzag ribbon, the realization of a spin/valley filter or diode, transport in full-time Floquet theory, and an alternative system to realize the SVP-QAH effect.

[33] T. Kitagawa, T. Oka, A. Brataas, L. Fu, and E. Demler, Phys. Rev. B **84**, 235108 (2011).

[34] M. Ezawa, Phys. Rev. Lett. **110**, 026603 (2013).

[35] Y.-W. Son, M. L. Cohen, and S. G. Louie, Nature (London) **444**, 347 (2006).

[36] X. Zhai and G. Jin, Phys. Rev. B **89**, 085430 (2014).

[37] S. Datta, *Electronic Transport in Mesoscopic Systems* (Cambridge University Press, Cambridge, England, 1995).

[38] X. Zhai, R. Wen, X. Zhou, W. Chen, W. Yan, L.-Y. Gong, Y. Pu, and X. Li, Phys. Rev. Appl. **11**, 064047 (2019).

[39] C. Gong and X. Zhang, Science **363**, eaav4450 (2019).

[40] P. Wei, S. Lee, F. Lemaitre, L. Pinel, D. Cutaia, W. Cha, F. Katmis, Y. Zhu, D. Heiman, J. Hone, J. S. Moodera, and C.-T. Chen, Nat. Mater. **15**, 711 (2016).

[41] Z. Sun, Y. Yi, T. Song, G. Clark, B. Huang, Y. Shan, S. Wu, D. Huang, C. Gao, Z. Chen, M. McGuire, T. Cao, D. Xiao, W.-T. Liu, W. Yao, X. Xu, and S. Wu, Nature (London) **572**, 497 (2019).

[42] B. Huang, J. Cenker, X. Zhang, E. L. Lay, T. Song, T. Taniguchi, K. Watanabe, M. A. McGuire, D. Xiao, and X. Xu, Nat. Nanotechnol. **15**, 212 (2020).

[43] A. Kundu, H. A. Fertig, and B. Seradjeh, Phy. Rev. Lett. **113**, 236803 (2014).

[44] H. Dehghani, T. Oka, and A. Mitra, Phys. Rev. B **91**, 155422 (2015).

[45] F. Manghi, M. Puviani, and F. Lenzini, Adv. Condens. Matter Phys. **2018**, 5703197 (2018).

[46] K. F. Mak, M. Y. Sfeir, Y. Wu, C. H. Lui, J. A. Misewich, and T. F. Heinz, Phys. Rev. Lett. **101**, 196405 (2008).

[47] L. E. F. Foa Torres, P. M. Perez-Piskunow, C. A. Balseiro, and G. Usaj, Phys. Rev. Lett. **113**, 266801 (2014).

[48] M. A. Sentef, M. Claassen, A. F. Kemper, B. Moritz, T. Oka, J. K. Freericks, and T. P. Devereaux, Nat. Commun. **6**, 7047 (2015).

[49] Y. H. Wang, H. Steinberg, P. Jarillo-Herrero, and N. Gedik, Science **342**, 453 (2013).

[50] J. Zhang, B. Zhao, T. Zhou, Y. Xue, C. Ma, and Z. Yang, Phys. Rev. B **97**, 085401 (2018).

[51] A. M. Tokmachev, D. V. Averyanov, O. E. Parfenov, A. N. Taldenkov, I. A. Karateev, I. S. Sokolov, O. A. Kondratev, and V. G. Storchak, Nat. Commun. **9**, 1672 (2018).